Monthly Notices
of the
ROYAL ASTRONOMICAL SOCIETY

MNRAS **451,** 3857–3867 (2015) doi:10.1093/mnras/stv1216

Sco X-1 revisited with *Kepler*, MAXI and HERMES: outflows, time-lags and echoes unveiled

S. Scaringi,[1]★ T. J. Maccarone,[2] R. I. Hynes,[3] E. Körding,[4] G. Ponti,[1] C. Knigge,[5] C. T. Britt[2] and H. van Winckel[6]

[1]*Max Planck Institute für Extraterrestriche Physik, D-85748 Garching, Germany*
[2]*Department of Physics, Texas Tech University, Box 41051, Lubbock, TX 79409-1051, USA*
[3]*Department of Physics and Astronomy, Louisiana State University, Baton Rouge, LA 70803-4001, USA*
[4]*Department of Astrophysics/IMAPP, Radboud University Nijmegen, PO Box 9010, NL-6500 GL Nijmegen, the Netherlands*
[5]*School of Physics and Astronomy, University of Southampton, Hampshire SO17 1BJ, UK*
[6]*Instituut voor Sterrenkunde, KU Leuven, Celestijnenlaan 200D, B-3001 Heverlee, Belgium*

Accepted 2015 May 28. Received 2015 May 21; in original form 2015 March 30

ABSTRACT

Sco X-1 has been the subject of many multiwavelength studies in the past, being the brightest persistent extrasolar X-ray source ever observed. Here, we revisit Sco X-1 with simultaneous short cadence *Kepler* optical photometry and Monitor of All-sky X-ray Image X-ray photometry over a 78 d period, as well as optical spectroscopy obtained with High Efficiency and Resolution Mercator Echelle Spectrograph (HERMES). We find Sco X-1 to be highly variable in all our data sets. The optical fluxes are clearly bimodal, implying the system can be found in two distinct optical states. These states are generally associated with the known flaring/normal branch X-ray states, although the flux distributions associated with these states overlap. Furthermore, we find that the optical power spectrum of Sco X-1 differs substantially between optical luminosity states. Additionally we find rms–flux relations in both optical states, but only find a linear relation during periods of low optical luminosity. The full optical/X-ray discrete correlation function displays a broad ≈12.5 h optical lag. However, during the normal branch phase, the X-ray and optical fluxes are anticorrelated, whilst being correlated during the flaring branch. We also performed a Cepstrum analysis on the full *Kepler* light curve to determine the presence of any echoes within the optical light curve alone. We find significant echo signals, consistent with the optical lags found using the discrete cross-correlation. We speculate that whilst some of the driving X-ray emission is reflected by the disc, some is absorbed and re-processed on the thermal time-scale, giving rise to both the observed optical lags and optical echoes.

Key words: accretion, accretion discs – X-rays: binaries – X-rays: individual: Sco X-1.

1 INTRODUCTION

Scorpius X-1 (hereafter Sco X-1) is a low-mass X-ray binary (LMXB), where a secondary main-sequence star transfers material on to a magnetized neutron star (NS) via Roche lobe overflow through an accretion disc. Sco X-1 was the first, persistently bright, extrasolar X-ray source to be discovered (Giacconi et al. 1962). It lies at a distance of 2.8 kpc (Bradshaw, Fomalont & Geldzahler 1999), has an orbital period of 18.9 h (Cowley & Crampton 1975; Gottlieb, Wright & Liller 1975; Hynes & Britt 2012), and contains a 0.4 $M_\odot$ M-type companion (Steeghs & Casares 2002). Since its discovery, many studies have been pursued on Sco X-1, all revealing its highly variable nature across the electromagnetic spectrum (see e.g. Mook et al. 1975; Hertz et al. 1992; Dieters & van der Klis 2000). In particular, Sco X-1 is a member of a group of objects called Z-sources. The class name arises due to the fact that apparent Z-shaped tracks appear when soft X-ray colours are plotted against hard X-ray colours. Many multiwavelength studies have been pursued on Z-sources in the past, revealing how the mass accretion rate, ultraviolet line and continuum fluxes and optical brightness are all correlated with where the sources lie on the Z-track (Hasinger et al. 1990; Vrtilek et al. 1990, 1991; Hertz et al. 1992). The topmost portion of the Z-track is referred to as the horizontal branch (HB), and systems have been shown to be rarely found in this state. As the sources progress downwards, they enter the normal branch (NB), whilst during episodes of higher X-ray flux, they enter the bottom part of the Z-track called the flaring branch (FB). In the case of

★ E-mail: simo@mpe.mpg.de

Sco X-1, the HB is far less pronounced than either the NB or FB. Additionally to X-ray colour changes, the X-ray power spectral density (PSD) of Sco X-1 displays clear quasi-periodic oscillations (QPOs), which appear to increase in frequency as the source moves downwards along the NB (van der Klis et al. 1996).

One of the first models invoked to explain the Z-track phenomenology was that of Priedhorsky et al. (1986) and Psaltis, Lamb & Miller (1995). In that model most of the X-ray emission originates from the NS magnetosphere, the hot central corona, and an extended corona through which material falls radially towards the NS. Variations within the Z-track then reflect variations in the mass accretion rate which varies between 0.5–1.1 times the Eddington critical rate, $\dot{M}_{\rm E}$. During low accretion rate episodes, Sco X-1 is found in the NB and moves downwards as $\dot{M}$ increases. This causes increased radiation pressure allowing material to pile-up close to the NS. The optical depth then increases, causing more X-ray photons to be absorbed and re-emitted as optical photons. This phase is associated with an X-ray to optical anti-correlation (McNamara et al. 2003). As the source transitions between the NB and the FB, the mass accretion rate exceeds the critical Eddington rate, causing the mass flow to become chaotic with material in the disc flowing both radially inwards and outwards. As material keeps building up in the outer corona the electron scattering opacity increases, redirecting some of the X-ray emitted photons on to the accretion disc. Contrary to the NB phase, the FB phase produces correlated X-ray and optical fluxes.

Recently, a different model has been proposed based on the idea of an extended accretion disc corona (ADC; Church & Balucinska-Church 1995; Church & Bałucińska-Church 2004; Church et al. 2012). In this model, $\dot{M}$ increases as the source moves upwards along the NB track (the opposite of the Psaltis et al. 1995 model). Although qualitatively different, this would still predict an X-ray/optical anti-correlation due to increased optical depths with higher accretion rates. Furthermore, movements along the FB away from the NB/FB vertex are also associated with increased $\dot{M}$, but here the flaring behaviour is associated with unstable nuclear burning on the NS surface (Church et al. 2012). The $\dot{M}$ increase along the FB is, however, only a property of Sco X-1 like sources: other systems like Cyg X-2 are instead thought to have constant $\dot{M}$ along the FB. Thus, given that most of the X-ray radiation is released from the NS rather than the disc, we might also expect that this scenario would produce correlated X-ray and optical fluxes as in the previous model. Furthermore, as movements along both FB and NB branches are associated with increased mass-transfer rates (and thus increased radiation pressure), the model predicts that both should display jet-launching. Indeed both branches have been shown to display radio emission, although the NB is more radio-loud than the FB (Hjellming et al. 1990).

Bradshaw, Titarchuk & Kuznetsov (2007) have studied the correlations between the X-ray spectral characteristics and QPOs in Sco X-1. They found a strong correlation between the kHz QPOs and the spectral power-law index and interpret this as being due to changes in the geometrical configuration of the corona. The same study shows how the equivalent width (EW) of the iron Kα emission line is anti-correlated with spectral hardness. The increase in EW implies a stronger accretion disc wind, assuming the iron Kα line is generated in the wind itself.

With the aim of testing and refining the current models for Sco X-1, we revisit this system with simultaneous data obtained from the *K2* mission and the MAXI(Monitor of All-sky X-ray Image) instrument, augmented by ground-based optical spectroscopy obtained with High Efficiency and Resolution Mercator Echelle Spectrograph (HERMES). Our data reduction procedures are described in Section 2, whilst our results are presented in Section 3. Our discussion, together with interpretation of our results, is discussed in Section 4, whilst our conclusions are drawn in Section 5.

2 DATA REDUCTION AND ANALYSIS

In this section, we present the three data sets used in this work (*K2*, MAXI, HERMES), and describe any relevant data reduction procedures employed.

2.1 *K2* light curve

The *NASA Kepler* mission was successfully launched on 2009 March 7. It continuously pointed towards the same 116 deg^2 field of view (FOV) during the entire mission, and obtained light curves with a 58.8 s cadence (short cadence, SC) or with a 30 min cadence (long cadence, LC) during every quarter (Q) of observations (Borucki et al. 2010). In 2013 May, *Kepler* entered a prolonged safe mode due to a second reaction wheel failure. Since then the mission has been re-purposed as the *K2* mission, covering new areas of the sky with the same SC and LC modes and the same FOV size. *K2* thus stares for 3 months at the same field before moving on to the next one. Although *K2* is not able to obtain year-long light curves as the original *Kepler* mission, it does allow us to study the timing properties of a wider range of astrophysical objects as the mission sweeps through the so-called *Kepler* ecliptic plane.

Sco X-1 was observed by the *K2* mission during Campaign 2 between 2014 August 23 and November 13 (78.8 d), and is the first ever LMXB to be observed with *Kepler*. Sco X-1 has a registered *Kepler* magnitude (*Kp*) of 12.4 in the *K2* Ecliptic Plane Input Catalog (EPIC). Here, we analyse SC data (cadence of 58.8 s) obtained from the Mikulski Archive for Space Telescope (MAST) archive.[1] The data is provided in raw format, consisting of target pixel data. For each 58.8 s exposure, we thus have a 14 $\times$ 12 pixel image centred on the target. Sco X-1 was near the edge of module 15.3. Although this module is not known to be affected by Moire Pattern Drift (MPD) noise the target point spread function (PSF) is asymmetric as it lies at the edge of one of the outermost modules. As no other sources were present within the 14 $\times$ 12 pixel images, we created the light curve by manually defining a large target mask as well as a background mask. A large target mask is required due to occasional small-scale jittering of the spacecraft, resulting in the target moving slightly from its nominal position. Fig. 1 shows the average target pixel image obtained from 115 679 individual target images. We removed 1919 observations because of bad quality due to occasional spacecraft rolls or due to cosmic rays. Fig. 1 also shows in red the target mask and in black the background mask. We produce the light curve by summing together all target pixels for each exposure, and subtract the average background obtained from the background pixel mask. The obtained light curve is shown in the top panel of Fig. 2. We believe this is the best ever optical light curve obtained for an LMXB in terms of timespan, cadence and photometric quality. A Fourier transform of the whole light curve reveals the orbital period at 18.9 h (see Fig. 3).

2.2 MAXI light curve

Since the MAXI (Matsuoka et al. 2009) experiment on-board the International Space Station (ISS) started in 2009 August, the GSC

[1] http://archive.stsci.edu/k2/

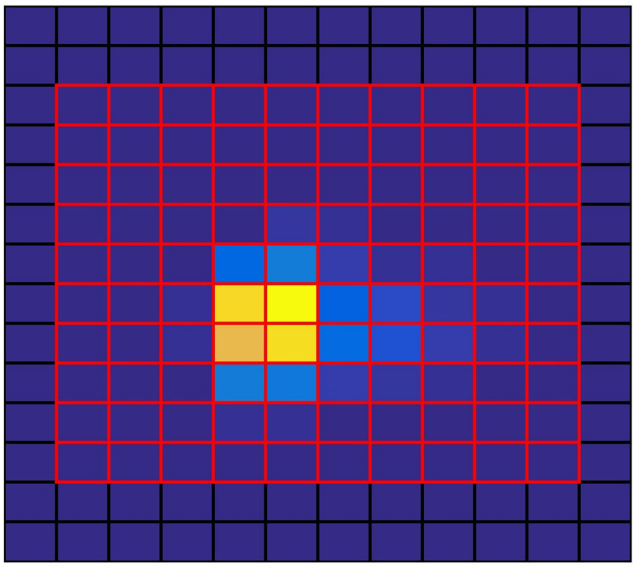

Figure 1. *K2* average target pixel image for Sco X-1. The target mask pixels are marked in red, whilst background mask pixels are marked in black.

(Gas Slit Camera; Mihara et al. 2011; Sugizaki et al. 2011), one of the two MAXI detectors, has been scanning almost the whole sky every 92-min orbital cycle in the 2–30 keV band. Here, we use the MAXI light curve of Sco X-1 during the period when the system was also observed by the *K2* mission. We obtained the light curve through the MAXI web site,[2] which provides reduced light curves in the three energy ranges 2–4, 4–10 and 10–20 keV. The combined light curve is shown in the bottom panel of Fig. 2. The corresponding X-ray colour–colour diagram is shown in Fig. 4, clearly displaying the NB/FB dichotomy.

2.3 Mercator/HERMES spectra

We observed Sco X-1 with the HERMES spectrograph (Raskin et al. 2011) mounted on the 1.2 m Mercator Telescope at La Palma, Canary Islands, Spain. This highly efficient echelle spectrograph has a resolving power of $R = 86\,000$ over the range 3800–9000 Å. Each spectrum was obtained from a 45 min exposure. The raw spectra were reduced with the instrument-specific pipeline, but are not flux-calibrated. In total we obtained six spectra at the times marked with the vertical dashed lines in Fig. 2. Here, we specifically examine the evolution of the six emission lines H α 6563, H β 4861, He I 5876, He I 6678, He I 7065 and He II 4685 Å. To do this, we normalize each line with an estimate of the neighbouring continuum. For each line, we iteratively fit a first degree polynomial around 40 Å of the desired line centre using sigma-clipping. We found this to converge after about five iterations. In cases where no evident emission line was present, the iterative sigma-clipping procedure excluded ≈3 per cent of data, whilst in cases where clear emission lines were present it excluded ≈15 per cent. The resulting normalized line profiles are shown in Fig. 5, together with their measured EWs.

3 RESULTS

In this section, we investigate the properties of Sco X-1 in the context of its NB and FB track dichotomy. We will determine what method best separates the two tracks using the *K2* and MAXI data sets and present average PSDs for the low and high optical luminosity states. This section additionally presents the results of cross-correlating the MAXI and *K2* light curves, the Cepstrum analysis to detect possible echoes in the *K2* light curve, as well as our optical spectroscopy campaign results.

3.1 NB and FB properties

Fig. 6 shows the optical flux distribution obtained from the *K2* light curve (left-hand panel, grey line) and the X-ray flux distribution obtained from the MAXI light curve (right-hand panel, grey line). The *K2* flux distribution is clearly bimodal, and possibly the MAXI fluxes as well. From the flux distributions alone it is not clear whether the bimodality is caused by the NB/FB dichotomy. To determine whether this is the case we performed principal component analysis (PCA) decomposition on the MAXI X-ray colours shown in Fig. 4 in order to determine which observations belong to which Z-track branch. Fig. 7 shows the obtained PCA projection. By using principal component 2 (*PC*2), we can clearly separate the NB from the FB. We employ conservative ranges to exclude transition data points and select FB MAXI observations as having $PC2 > 0.2$ and NB MAXI observations as having $PC2 < -0.2$. The resulting X-ray flux distributions for both the NB and FB obtained from our selected points are shown in Fig. 6. Although NB X-ray fluxes seem to only populate the low-flux distribution in Fig. 6, the FB fluxes seem to populate both distributions. Thus, X-ray fluxes alone are not a good discriminator between NB/FB tracks. We then located all *K2* observations that lie within ±45 min from the MAXI observations (MAXI data points have a cadence of one ISS orbit, or 1.5 h). The resulting FB and NB flux decomposition from our PCA projection is also shown in Fig. 6. It is clear that in the absence of X-ray colour information, optical fluxes are better than X-ray fluxes in distinguishing between NB and FB. However, we point out that optical fluxes alone are also not good indicators of the NB/FB dichotomy, given the long tails displayed in Fig. 6.

Given the optical flux bimodality, we decided to produce broad-band PSDs from the *K2* light curve for different flux levels. We selected conservative ranges to avoid the transition region, and chose to call low optical luminosity observations all data lying below 4.6×10^4 e$^-$ s^{-1} and high optical luminosity those lying above 5.6×10^4 e$^-$ s^{-1}. These limits are marked with vertical lines in Fig. 8. We then computed 1-d, non-overlapping PSDs (78 of them), and produced a low-luminosity PSD by averaging 30 of them whose mean fluxes lay within the optical flux range shown in Fig. 8. The high optical luminosity PSD was similarly obtained by averaging 28 PSDs. The logarithmically binned result of this procedure is shown in Fig. 9. At first look it is already clear that the PSD shapes differ substantially between the low and high optical luminosity states. We include in Fig. 9 a dashed grey line showing a power law with a −2 gradient for comparison. During both high and low optical luminosity states the PSDs appear to follow a general −2 power-law shape. At low optical luminosities, the PSD possibly displays an additional noise component around $\approx 2 \times 10^{-4}$ Hz. On the other hand during high optical luminosities a clear broad-noise component is observed in addition to the general ≈−2 power-law slope, peaking around $\approx 10^{-3}$ Hz. The flattening observed at the highest frequencies is probably due to instrumental noise. It is clear that the PSD phenomenology is quite complex and differs substantially between states. A detailed modelling in terms of power laws and Lorentzian components is beyond the scope of this work and will be addressed in future.

[2] http://maxi.riken.jp

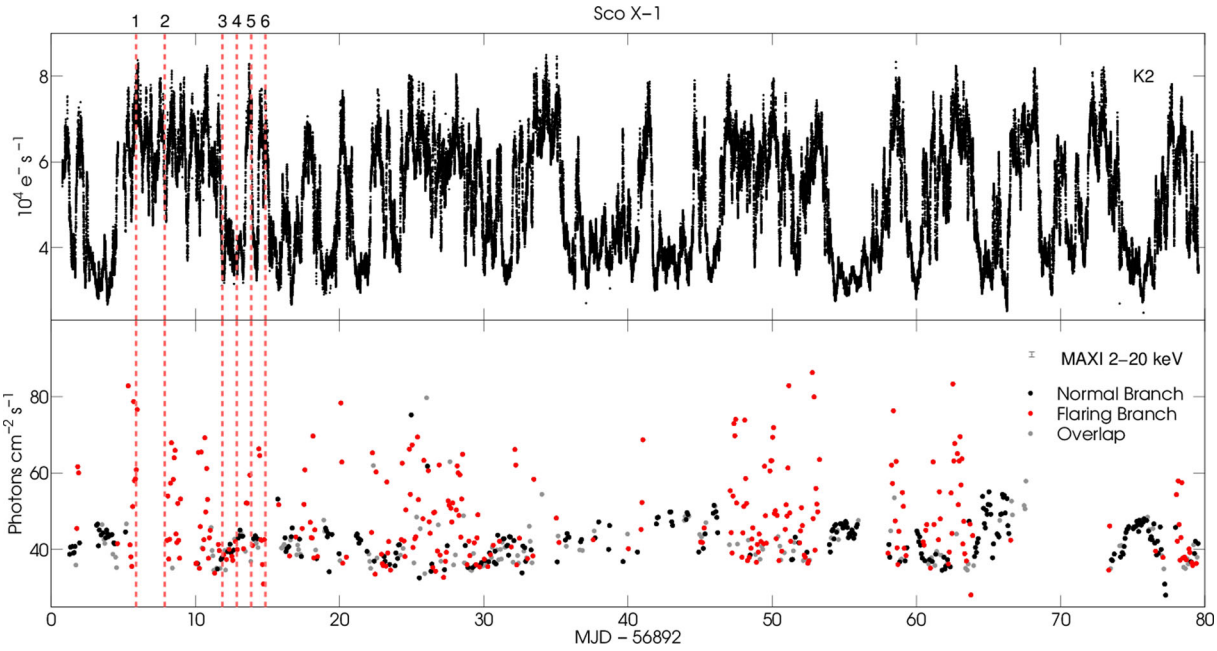

Figure 2. Top panel: *K2* Sco X-1 light curve. The system was observed for over 78 d at 58.8 s cadence. The units on the *y*-axis are electrons /second, and can be converted to *Kepler* magnitudes *Kp* using the conversion found in the *Kepler* Instrument Handbook. Bottom panel: 2–20 keV MAXI light curve during the same period. Data points are colour coded using the NB/FB decomposition shown in Fig. 7. Typical MAXI error bar is shown on the top-right. The vertical dashed lines mark the times of our HERMES observations.

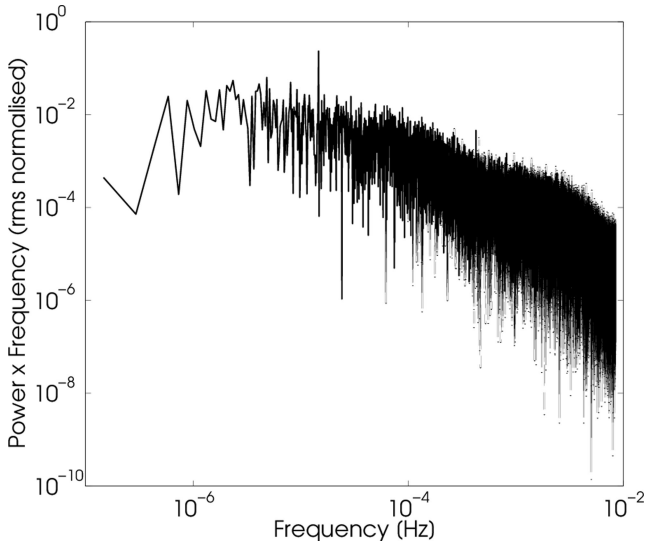

Figure 3. Fourier transform of the full 78.8 d SC *K2* data for Sco X-1, showing a clear peak at the orbital period of 18.9 h.

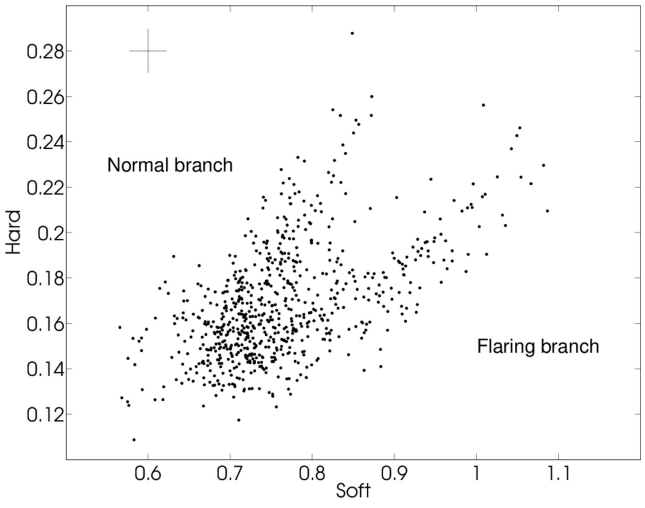

Figure 4. Sco X-1 colour–colour X-ray diagram obtained from MAXI data. The soft colour is defined as the ratio of 4–10 keV/2–4 keV, whilst the hard colour is defined as the ratio of 10–20 keV/4–10 keV. Typical error bar shown on the top-left.

Using the optical flux limits defined in Fig. 8, we are also able to produce root-mean-square versus flux (rms–flux) relations for both the low and high optical luminosity states. This was done by computing mean fluxes and rms values for all non-overlapping 5-min data segments, excluding any data gaps caused by the flux limit selections. Fig. 10 shows our binned results. In the low-luminosity state, an rms–flux relation consistent with linearity is obtained. In the high-luminosity state, it appears that linearity is broken at the highest fluxes. This could be suggestive that an additional flux distribution exists at the highest fluxes, thus making the light curve non-stationary and breaking the rms–flux linearity. We note that this could be connected to the trimodal flux distribution previously reported in Sco X-1 (Mook et al. 1975; McNamara et al. 2003) and/or the extra variability component observed during the high optical luminosity state as seen in Fig. 9. A similar property might also be observed in the NS XRB PSR J1023+0038 (Bogdanov et al. 2014), although we caution the reader that this particular system might have a higher accretion rate that Sco X-1, and thus any phenomenological similarity in the flux distributions might be coincidental. Nevertheless, it would be interesting to establish whether the rms–flux relation holds its linearity for this system or whether it breaks down at high fluxes as seen in Sco X-1. We also note that at the lowest fluxes the high optical luminosity rms–flux relation gradient is higher compared to the low-luminosity one.

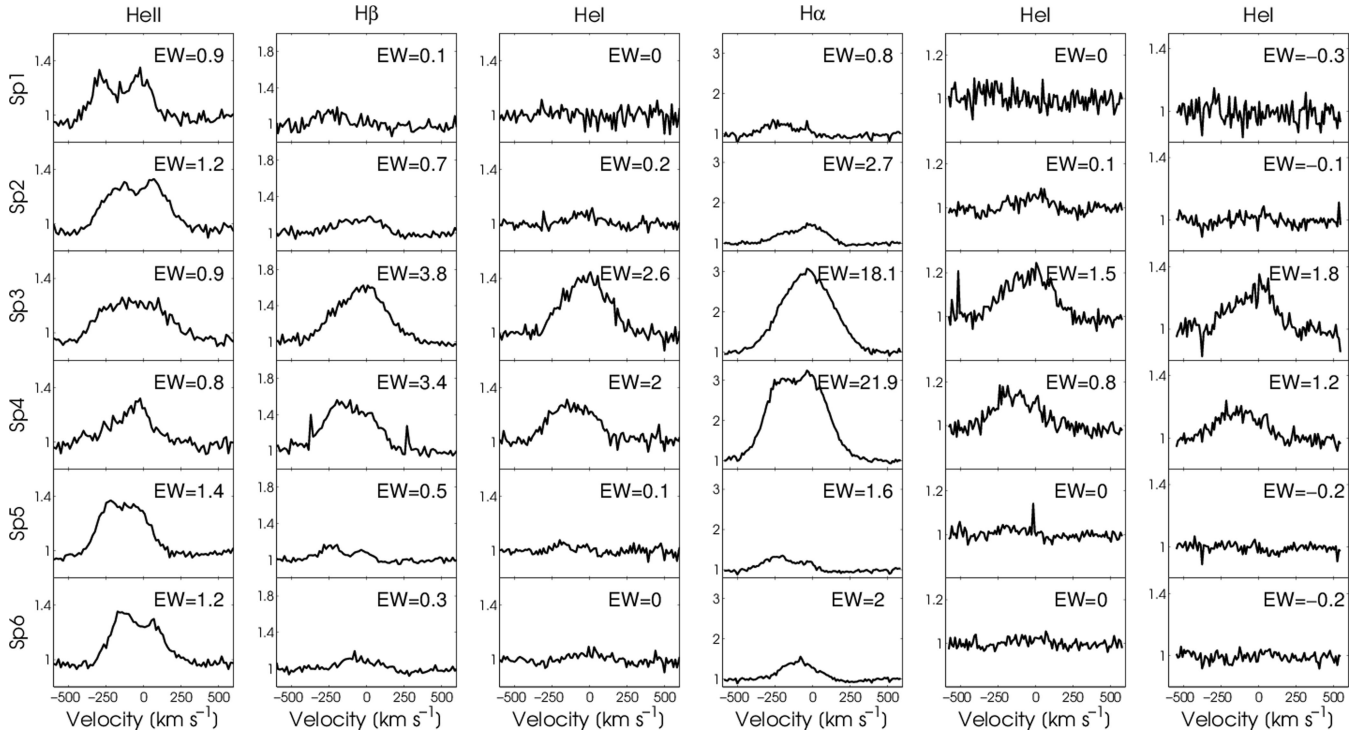

Figure 5. HERMES spectra normalized to continuum. Each row is one observation taken at times marked in Fig. 2 with vertical dashed red lines. Columns are different zooms around different emission lines. Each panel also shows the measured EW of the lines. Note the increased line EW when Sco X-1 was in its NB state (Spectra 3 & 4).

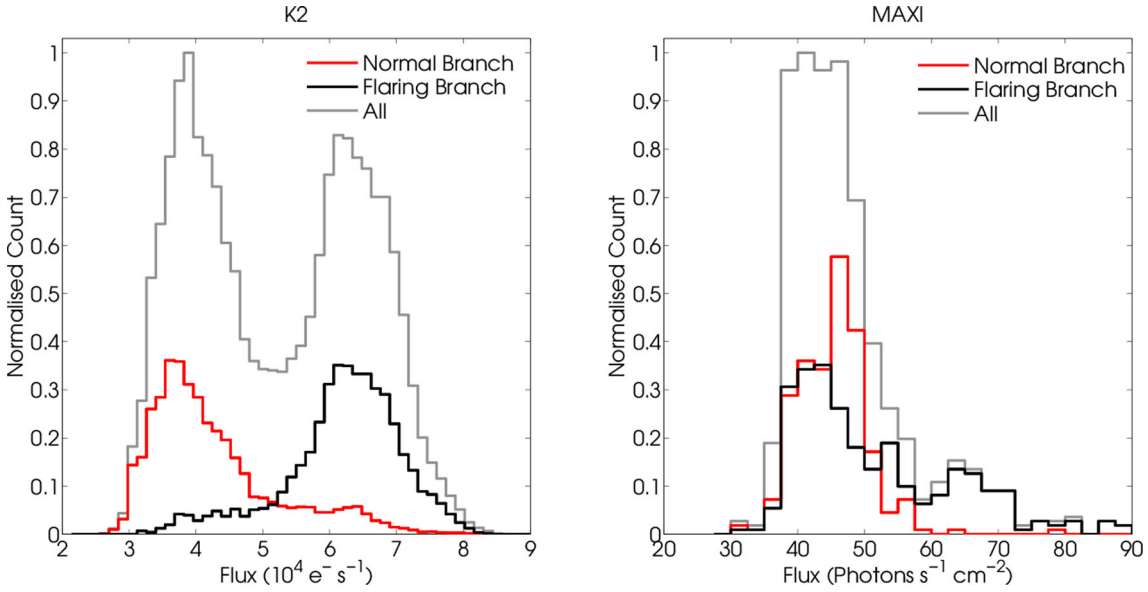

Figure 6. Left-hand panel: *K2* flux distribution decomposed using PCA as applied to X-ray colours. Note that due to the conservative range employed the FB and NB, data points are not all recovered. Right-hand panel: MAXI flux distribution decomposed using PCA as applied to the corresponding X-ray colours.

Fig. 5 shows the six spectra obtained with the HERMES spectrograph. Each column shows six different continuum normalized emission lines. The low-ionization emission lines of H α, H β and He I qualitatively appear to have larger EWs during periods of low optical luminosity (Spectra 3 & 4) compared to the high luminosity spectra. On the other, hand, the EW of the higher ionization He II line does not appear to change by much. Furthermore, He II appears to be double-peaked only during the high optical luminosity states phase. Possible explanations for this qualitative behaviour will be discussed in Section 4.

3.2 X-ray lags & optical echoes

We computed the discrete cross-correlation function (DCF, Edelson & Krolik 1988) between the *K2* and MAXI 2–20 keV light curves using a time step of 45 min (half the MAXI cadence). The results are

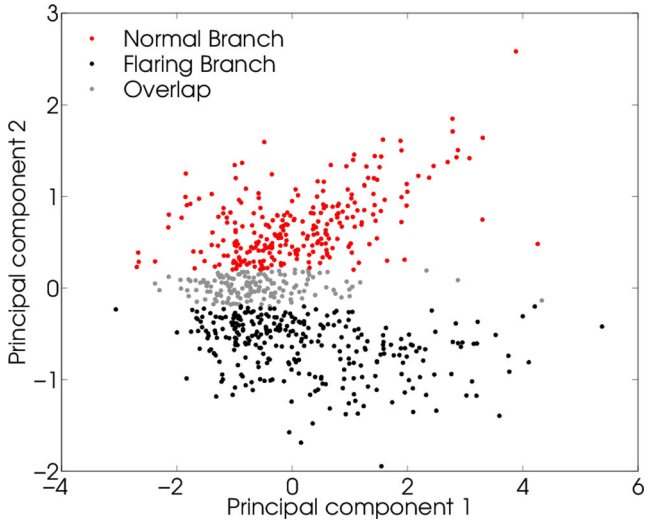

Figure 7. Projected hard and soft X-ray colours using PCA. We define conservative regions for the FB and NB by selecting MAXI observations that lie 0.2 above/below *PC*2.

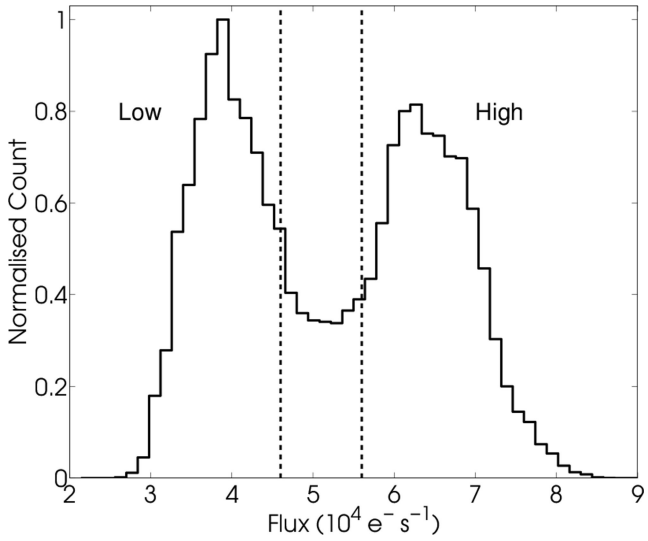

Figure 8. Sco X-1 optical flux distribution obtained with *K2*. The vertical lines correspond to conservative boundaries for low and high optical luminosity states determined by eye.

shown in Fig. 11 where the *x*-axis is optical lag in units of hours. We further computed confidence levels by simulating 10^5 light curves on the same *K2* sampling pattern of the original data. Each light curve was simulated using the Timmer & Koenig (1995) algorithm. As we do not have an analytical model for the intrinsic PSD of Sco X-1 within the frequency range of interest, we produced the input PSD by first computing the full Fourier transform of the original *K2* data and smoothing it with a 50-point moving average. The dashed line in Fig. 11 shows the obtained 3σ (99.7 per cent) contour level from our Monte Carlo simulation.

A clear significant zero-lag peak is evident. Given our timing resolution, this peak is consistent with the finding that the optical light curve lags the X-ray light curve by tens of seconds due to reprocessing from the secondary star and/or accretion disc (Muñoz-Darias et al. 2007; Britt 2013). Additionally the DCF is very asymmetric, with a second broad significant bump around 12.5 h. This time-scale

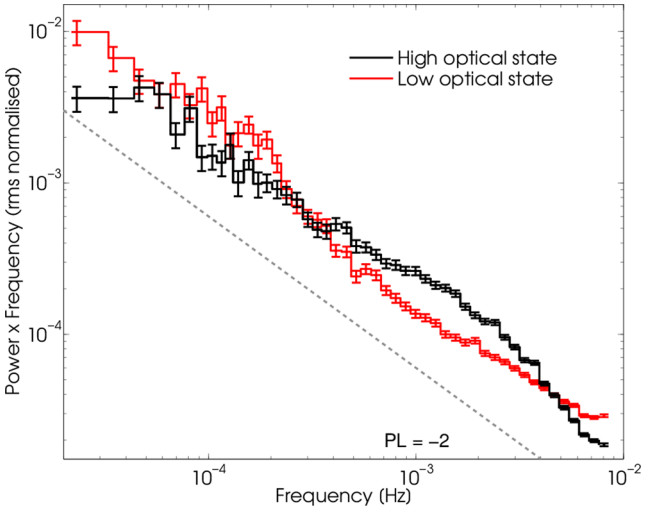

Figure 9. PSDs obtained from the low and high optical luminosity intervals defined from the flux distribution shown in Fig. 8. The dashed grey line shows a −2 power law for comparison.

might be consistent with the disc thermal time-scale, and will be discussed further in Section 4.

Motivated by the different properties between the NB and the FB, as well as the idea that X-ray/optical light curves should be anticorrelated in the NB, we further computed the DCF for the two separate populations. We used the full *K2* light curve for both, and selected MAXI data segments using the PCA decomposition shown in Fig. 7. The results of this are shown in Fig. 12, where the contour levels have been computed in the same way as for the whole data set of Fig. 11. Although slightly more scattered, the DCFs for the individual NB and FB show different qualitative behaviour. Similarly to the full data set DCF, the FB DCF is asymmetric in the same direction. It displays a positive peak at zero time-lag, and although marginally significant, a potential secondary optical lag peak at ≈4.5 h. During the NB the two light curves are anticorrelated and appear more symmetric than for the FB. This effect can also be noticed in the light curves themselves by close visual inspection (see e.g d ≈75 in Fig. 2). The correlation/anticorrelation properties between X-ray and optical fluxes have been already reported in the past (McNamara et al. 2003) using X-ray flux versus optical flux plots, which we here confirm and characterize in more detail using the DCF. Fig. 13 shows our version of X-ray versus optical flux diagram, where we have additionally marked with circles the positions of when our optical spectra was taken. Simply from visual inspection it can be noticed that Spectrum 3 & 4 (which have the strongest emission lines) have been taken at times where the optical flux was lowest, but where the X-ray flux is not so different as for the other spectra. This suggests that low-ionization line strength is more strongly correlated to optical flux and not X-ray fluxes or colours.

Finally, we were also interested in determining whether the *K2* optical light curve alone displays any echoes. Any detection of such features would be interesting for a number of reasons. For example, if the optical lag (response) detected in Fig. 11 is associated with the disc thermal time-scale, we might expect an echo within the optical light curve alone around the same time. To determine whether any echoes are present in the *K2* light curve, we computed the so-called Cepstrum. The Cepstrum is computed as the inverse Fourier transform of the logarithm of the estimated spectrum of the light curve (see e.g. Bogert, Healy & Tukey 1963), Afraimovich 1981), and is

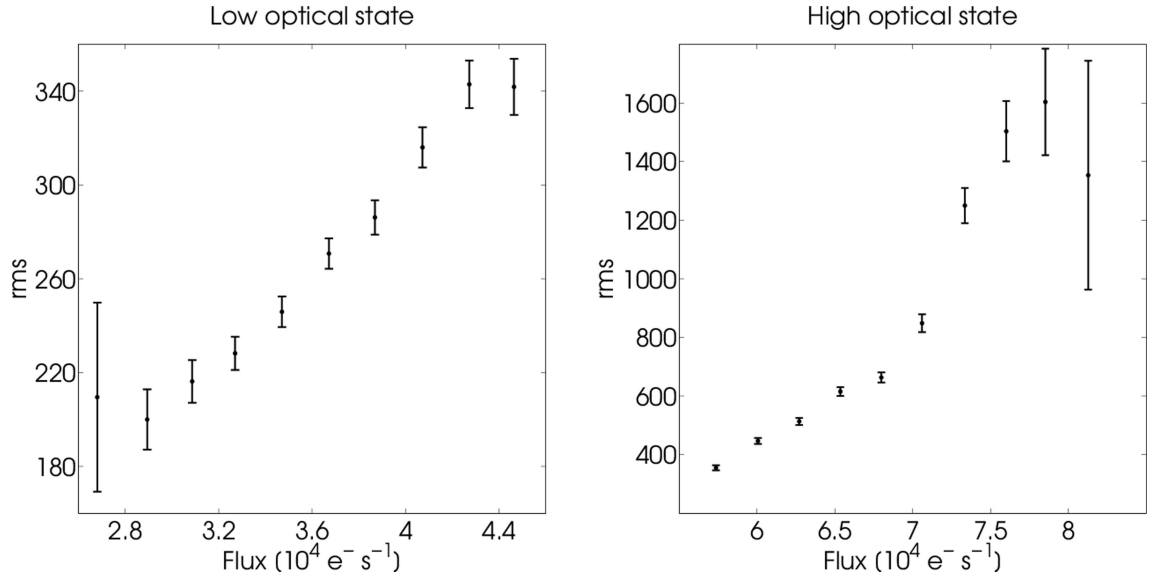

Figure 10. rms–flux relations obtained for Sco X-1 during low and high optical luminosity states selected using the regions defined in Fig. 8.

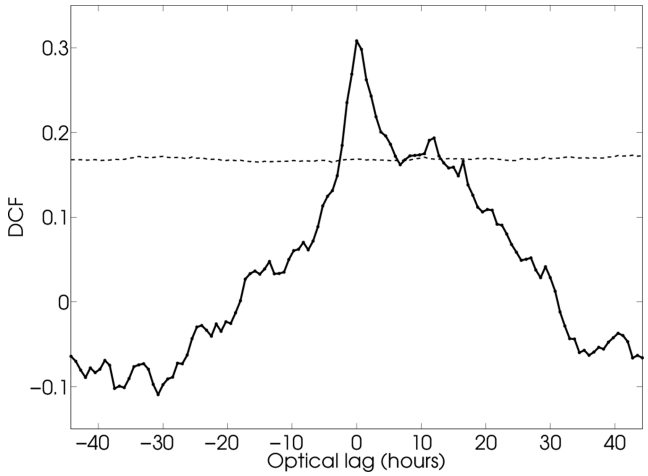

Figure 11. Discrete cross-correlation between MAXI and *K2* data (solid line) and 3σ detection level (dashed line).

used to find repeating signals (echoes) within a single time series. Confidence limits can also be computed with a similar method as that employed for the DCF confidence limits. We simulate 10^5 light curves using the same input PSD as previously adopted, and determine for each time-scale the 3σ level. The results of this is shown in Fig. 14. Three significant signals are detected at 1, 4.4 and 12.6 h. We will discuss possible mechanisms to generate these echoes in Section 4, but already note here that the signal at 12.6 h is consistent with the observed optical lag shown in Fig. 11, and that the 4.4 h signal is consistent with the FB DCF marginally detected secondary peak in Fig. 12. We also point out that the Cepstrum is solely based on the *K2* light curve, thus any matching signals between the Cepstrum and the DCFs are unlikely to be coincidental.

4 DISCUSSION

In this section, we discuss our findings in the context of the Church et al. (2012) model for Z-sources in general and Sco X-1 in particular. We also propose interpretations for several newly discovered phenomena.

4.1 X-ray and optical state properties

Phenomenologically, Sco X-1 transitions between NB and FB on time-scales of $\approx$1 d. According to Church et al. (2012) the proposed mechanisms for generating these transitions is related to the mass-transfer rate varying, such that $\dot{M}$ increases along both the FB and NB tracks away from the vertex. The X-ray colour changes reflect the relative contribution to the X-ray flux of the blackbody disc component (dominating in the soft X-ray band) and Comptonized corona (dominating in the hard X-ray band). As the optical emission is thought to originate from a colder outer disc, the optical flux distribution better tracks $\dot{M}$ changes, being unaffected by X-ray absorption and/or the X-ray contribution by different X-ray emitting components. Thus, although both the X-ray and optical flux distributions appear bimodal, the bimodality found in X-rays may not correspond simply to states with different $\dot{M}$.

One important consequence of the Church et al. (2012) model (but also the older Psaltis et al. 1995 model) is that as $\dot{M}$ increases, during the NB phase, the optical depth close to the NS also rises, due to higher radiation pressure. This might cause X-ray photons to be absorbed and re-emitted as optical photons, resulting in an anticorrelation between X-ray and optical fluxes. This is observed in Fig. 12. On the other hand, during the FB phase, the Church et al. (2012) model predicts an additional X-ray component caused by unstable nuclear burning on the NS surface. This additional X-ray component would shine on the optical emitting outer accretion disc, so we should observe a correlation between optical versus X-ray fluxes. This is also observed as shown in Fig. 12.

We have also found that the broad-band PSD shape of Sco X-1 differs substantially between the low and high optical luminosity states, with the latter displaying an additional broad-noise component breaking at $\approx 10^{-3}$ Hz superimposed ≈ -2 power law. Bildsten (1993) has previously reported that a possible time-dependent accretion regime exists in accreting NS, where small patches of the NS burn intermittently (unstable and persistent, as opposed to burning steadily or rapidly on the entire NS surface). The fire will then

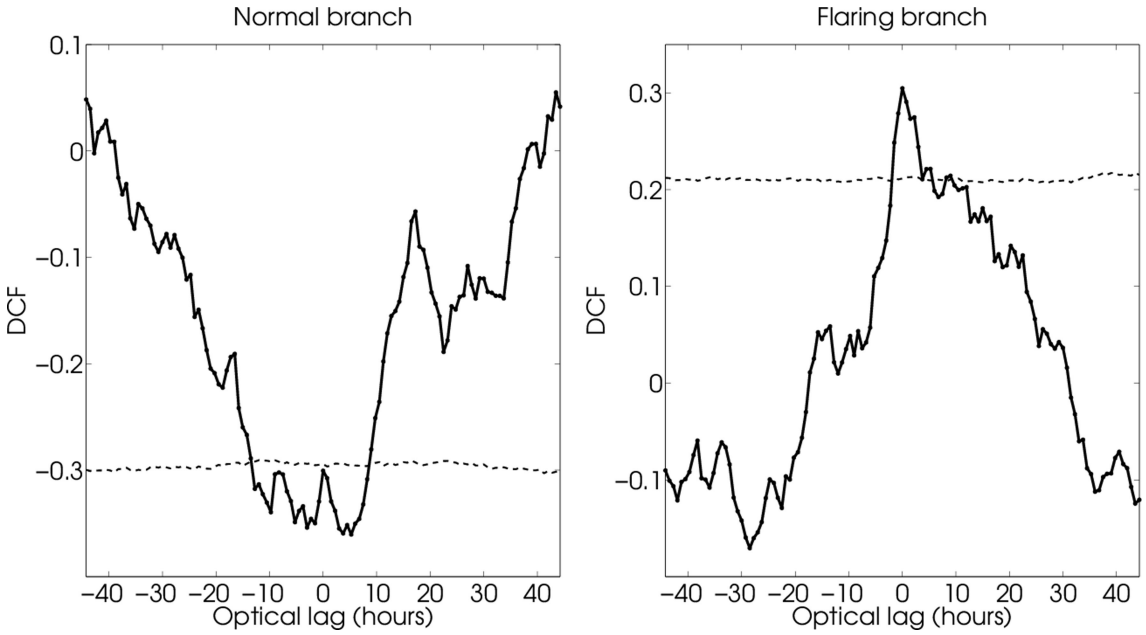

Figure 12. Discrete cross-correlation between MAXI and *K2* data selected according to the PCA decomposition for NB and FB (solid line, left and right, respectively). The dashed lines mark the 3σ detection levels.

propagate around the NS on the time-scale it takes to accrete enough fuel for the next instability, which lies in the range between 10^3 and 10^4 s. Thus, low-level luminosity variations should be observed on a similar frequency range. Indeed Hasinger & van der Klis (1989) have reported 'very low frequency' noise observed on similar time-scales. Given that the high optical luminosity state is somewhat associated with the FB for Sco X-1, and given that according to the Church et al. (2012) model this is where nuclear burning occurs on the NS surface, it is possible that the additional noise component in the high optical luminosity state observed here is in fact associated with the Bildsten (1993) mechanism.

It is also interesting to note how the rms–flux relations differ between the two low and high optical luminosity states. Linear rms–flux relations have been detected in all accreting compact objects (from Active Galactic Nuclei to accreting white dwarfs, see e.g. Uttley, McHardy & Vaughan 2005; Heil, Vaughan & Uttley 2012; Scaringi et al. 2012; Van de Sande, Scaringi & Knigge 2015). The general model invoked to explain the linear rms–flux relations is that of the fluctuating accretion disc model (Lyubarskii 1997; Kotov, Churazov & Gilfanov 2001; Arévalo & Uttley 2006). In this model, the observed variability is associated with modulations in the effective viscosity of the accretion flow at different radii. More specifically, the model assumes that, at each radius, the viscosity – and hence accretion rate – fluctuates on the local viscous time-scale around the mean accretion rate, whose value is set by what is passed inwards (again on the viscous time-scale) from larger radii. The overall variability of the accretion rate observed through light-curve variations is therefore effectively the product of all the fluctuations produced at larger radii. It is important to realize, however, that the detection of the rms–flux relation only suggests that the observed variability is the result of multiplicative processes (rather than additive) and does not necessarily rule out more complex (or less complex) accretion disc models to generate the observed variability.

In Sco X-1, the optical *K2* light curve does always exhibit a positive correlation between mean flux and rms. However, this correlation is only linear in the low optical luminosity state. This suggests that during low optical luminosities the light curve is indeed the result of multiplicative processes, which are possibly the result of a fluctuating accretion disc. During times of high optical luminosity, the rms–flux relation deviates from linearity (with an apparent change of slope to lower values) suggesting that more complex phenomena are at play during this phase. It is possible that the high optical luminosity state is composed of more than one accretion regime (for example the unstable nuclear burning mechanism of Bildsten 1993), causing the higher fluxes of this phase to be non-stationary with respect to the lower fluxes. Whatever the reason, it is interesting to note that multiplicative processes alone cannot reproduce non-linear rms–flux relations.

4.2 Optical spectroscopy

The HERMES spectra reveal that the low-ionization lines of H α, H β and He I appear stronger when Sco X-1 is in a low optical luminosity state (but not necessarily at low X-ray luminosities). Fender et al. (2009) have found a similar trend in a sample of XRBs, where an anticorrelation is found between the X-ray luminosity and the H α EW. Fender et al. (2009) suggest that the observed anticorrelation is the result of optical depth changes.

In Sco X-1, the anticorrelation could be due to the outer disc becoming cold and optically thin in the continuum, but not the emission lines, during the transition between the two optical luminosity states (Williams 1980; Fender et al. 2009). In this scenario, the optical continuum would drop much faster than the ionizing continuum produced in the inner disc regions. The EW of the optical lines produced in the outer disc should thus increase. The same would also hold during the opposite transition from low to high states, as the continuum would rise much faster than the emission lines, thus swamping them out and decreasing their measured EWs. Another possibility is that during the high optical luminosities most of the accretion disc becomes too hot for the production of low-ionization emission lines. This would not necessarily cause higher

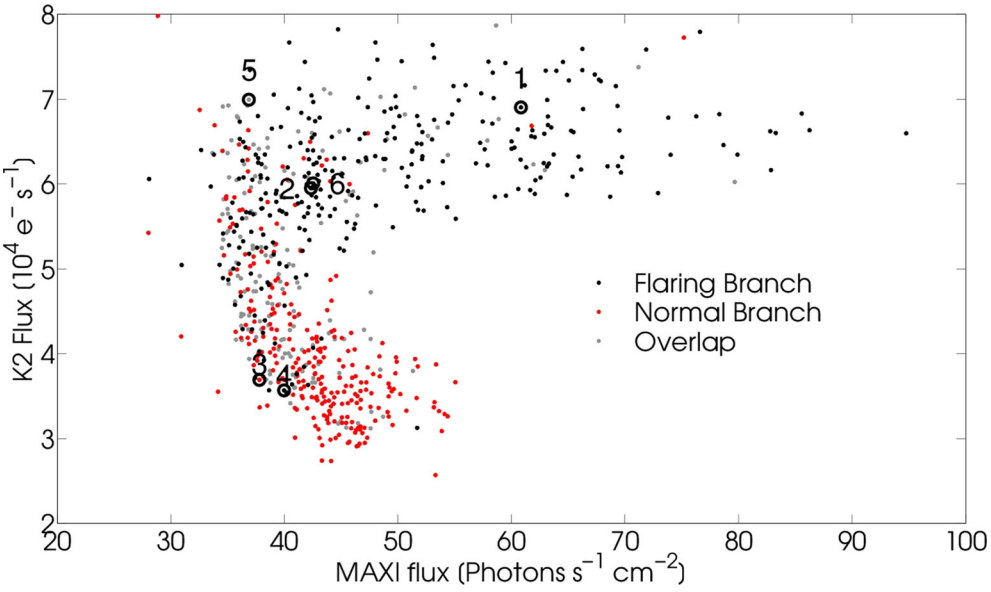

Figure 13. *K2* versus MAXI fluxes colour coded using the NB/FB PCA decomposition of Fig. 7. Circles indicate the time when the six HERMES spectra were obtained, numbered from 1 to 6 as in Fig. 5.

ionization lines such as He II to decrease in EW. In this case optical fluxes alone (rather than X-ray colours) would provide a better tracer for $\dot{M}$ changes in the optical emitting region. Indeed two of our six spectra with the lowest optical fluxes display the highest EWs. Furthermore, we do not measure significant changes in the He II EW, possibly making this scenario a more viable explanation.

Although the He II EW does not appear to significantly change between the low and high optical luminosity states, it does display a double-peaked profile only during low-luminosity ones. We note that the He II line profile changes do not appear to depend on the NB/FB dichotomy, but simply on optical luminosity (see Fig. 13). The change from double- to single-peaked profiles has been previously associated with the presence of outflows (see e.g. Murray & Chiang 1996). This deduction of a wind could potentially be consistent with the X-ray observations of the iron Kα emission line modelling in Sco X-1 (Bradshaw et al. 2007), which associates a strong wind to an X-ray softening.

4.3 X-ray time-lags and optical echoes

One other interesting feature is the broad ≈12.5 h optical lag shown in Fig. 11. Naively, from the fluctuating accretion disc model (Lyubarskii 1997; Kotov et al. 2001; Arévalo & Uttley 2006), we might have expected to observe an X-ray lag due to material propagating from an optical emitting region in the outer disc to an X-ray emitting region in the inner disc. Instead we observe the exact opposite for Sco X-1: first we observe X-rays and hours later the signal appears in the optical band. Given the hour-long measured time-scales in the cross-correlation function of Fig. 11, our result rules out light-travel time reverberation from the disc as a possible mechanism. We do not know at the time of writing what is the mechanism behind the observed optical lags but speculate that it could be the result of reprocessed X-ray photons to optical wavelengths on the disc thermal time-scale. This idea is not new, and has been invoked to explain Fourier-dependent time-lags observed in accreting white dwarfs (Scaringi et al. 2013).

Although the optical emission in the broad *Kepler* passband will originate from a large radial disc component, we can attempt to place constraints on α since the thermal time-scale $t_{\rm th} = \frac{1}{\Omega\alpha}$ (where Ω is the dynamical frequency at some given radius in the disc and α is the viscosity parameter of Shakura & Sunyaev 1973). Fig. 15 shows the obtained α values as a function of disc radius assuming a NS mass of 1.6 $M_\odot$ (Muñoz-Darias et al. 2007) by setting $t_{\rm th} = 12.5$ or $t_{\rm th} = 4.4$ h (two of the peaks detected in the Cepstrum analysis). The constraints obtained from Fig. 15 are physically plausible, suggesting that the measured lag time-scale could be associated with the disc thermal time-scale.

If the measured lags are really associated with the thermal time-scale we would expect the X-ray and optical variability to have a very small, light-travel time, lag which we observe in Fig. 11 as the strong zero-lag peak. As some X-ray radiation will be absorbed by the disc and re-emitted on the thermal time-scale at optical wavelengths we might then also expect a secondary, broad, optical lag peak. In this case, we might expect the optical light curve to also display an echo, since the same signal should appear twice within the light curve (once reflected and once reprocessed), with a delay close to $t_{\rm th}$. As one of the significant peaks found in the Cepstrum (Fig. 14) is similar to the measured broad X-ray lag, we tentatively associate this with the echo mechanism proposed above. A similar process might explain the other two detected echoes. In fact, the FB DCF in Fig. 12 is qualitatively similar to the full DCF of Fig. 11. Given our time resolution used to compute the DCFs, we would not be able to observe the 1 h cepstral peak in the DCFs. We point out that our Cepstrum analysis is based on the full 78-d *K2* light curve, and that we are not able at this time to localize the echoes within the light curve. Thus, multiple features in the Cepstrum do not necessarily need to occur at the same time within the 78-d period.

We caution at this stage that our tentative association of the optical lags and Cepstrum signals to the disc thermal time-scale are tentative, as they have never been observed on these time-scales. However, given the long time-scales involved, the non-detection of such lags in other similar systems is not surprising, since one would require continuous and long monitoring of XRBs at both X-ray and optical wavelengths. It is interesting to note the possibility that optical lags might only be detected in the FB state (since the NB shows X-ray/optical anticorrelation), and that the disc heating

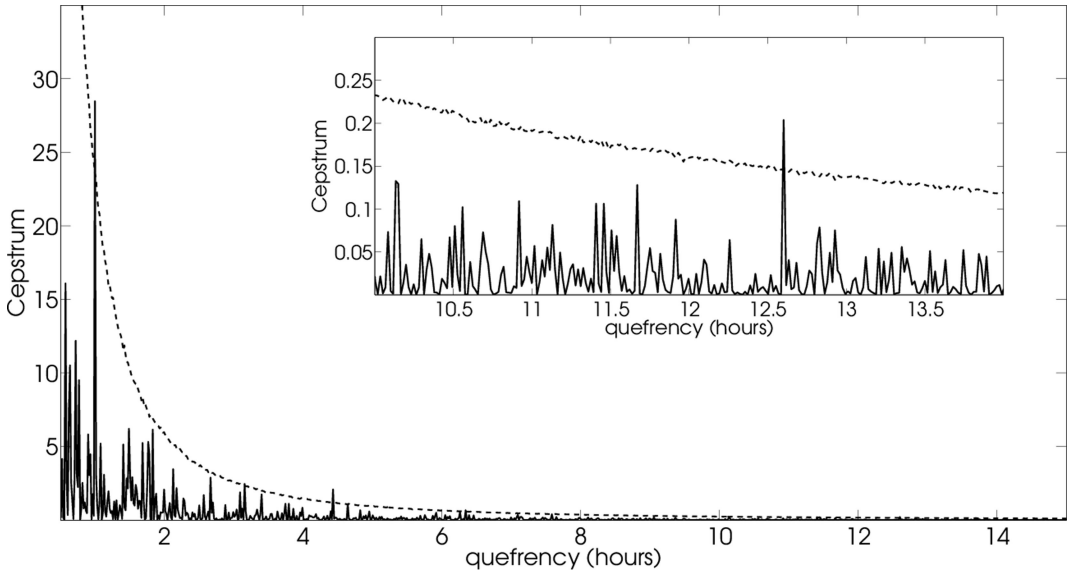

Figure 14. Cepstrum obtained from the *K2* light curve (solid line) and 3σ contour level (dashed line). The x-axis of the Cepstrum is referred to as the 'quefrency', and has units of time. Three significant peaks are detected at 1, 4.4 and 12.6 h.

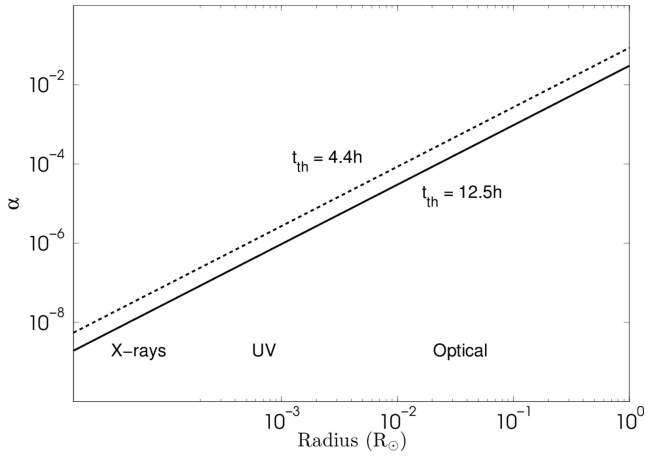

Figure 15. α dependence with disc radius for $t_{\rm th} \approx 12.5$ h (solid line) and $t_{\rm th} \approx 4.4$ h (dashed line). We also mark approximate radii regions of different electromagnetic emission.

mechanism could be driven by the unstable nuclear burning on the NS surface. A detailed study into whether this scenario is feasible for Sco X-1 is however beyond the scope of this paper.

5 CONCLUSION

A prime motivation for this study has been to revisit the well-known LMXB Sco X-1 with newly available data to test and refine the current physical model used to explain its phenomenological behaviour. Our data set comprises a continuous 58.8 s cadence light curve over more than 78 d obtained with the *K2* mission, and represents the best ever optical light curve obtained for an LMXB. We additionally used X-ray data obtained with the MAXI instrument on-board the ISS which provided us with X-ray light curves in the three energy bands 2–4, 4–10 and 10–20 keV over the same observing period of *K2*. Finally, we augmented our analysis with high-resolution optical spectroscopy taken during the same period with the HERMES instrument mounted on the 1.2 m Mercator telescope.

We can summarize the major findings of this paper as follows.

(i) In the absence of X-ray colours, optical fluxes have a greater discriminatory power in isolating the NB and FB phases than X-ray fluxes alone. However, even optical fluxes alone cannot properly separate the two phases.

(ii) The PSD of Sco X-1 appears to change in shape between low and high optical luminosity states. Qualitatively, the low-luminosity PSD can be expressed as a red noise PSD with a power law ≈ -2. During high optical luminosities, an additional component is observed on top of the power law with a possible break at $\approx 10^{-3}$ Hz. This additional broad-band feature could possibly be associated with unstable nuclear burning on the NS surface (Bildsten 1993).

(iii) Sco X-1 displays rms–flux relations in both the low and high optical luminosity states. However, a linear relation is only observed during low luminosities. The deviation from linearity, during high-luminosity states, might suggest that an additional variability component is present, thus removing the linearity and stationarity at the highest fluxes. This component could possibly be associated with the extra variability component observed in the FB PSD.

(iv) We find that the EWs of the low-ionization lines H α 6563, H β 4861, He I 5876, He I 6678 and He I 7065 Å are higher during times of lower optical luminosity, whilst He II 4685 Å does not appear to change in strength. This can be explained if during high optical luminosity periods (when $\dot{M}$ is highest) the accretion disc is too hot for the production of low-ionization lines, but not hot enough to remove higher ionization lines such as He II 4685 Å. We also find that He II 4685 Å appears to be double-peaked only during high optical luminosity states. It is possible that the single-peaked profile of He II 4685 Å is associated with an accretion disc outflow during the low optical luminosity phase. This interpretation is in line with previous X-ray measurements of the iron Kα emission line model (Bradshaw et al. 2007), where fast outflows are supposed to be generated in Sco X-1 during periods of high mass transfer.

(v) The DCF between the available optical *K2* and X-ray MAXI light curves displays clear asymmetry. The DCF profile displays a clear, broad, 12.5 h secondary optical lag peak. This can potentially be attributed to the disc thermal reprocessing time-scale.

(vi) The DCF obtained during the FB also displays clear asymmetry, and is qualitatively similar to the full DCF, with a secondary marginal detection of a 4.5 h optical lag peak. This too could potentially be the signature of the disc thermal time-scale. It is thus possible that the broad optical lags are mostly generated during the FB state.

(vii) The DCF obtained during the NB clearly show that the optical and X-ray variability are anticorrelated during this phase. This phenomenon has been previously reported by other authors.

(viii) We detect clear echoes within the optical *K2* light curve alone using the Cepstrum, at 1, 4.4 and 12.6 h. The 12.6 h echo time-scale is consistent with the full optical/X-ray DCF, whilst the 4.4 h echo is consistent with the FB DCF. Even if it were present in any of the DCFs studied here, we would not be able to recover the 1 h echo due to our DCF resolution. We interpret these echoes as the disc thermal time-scale, connected to the DCF optical lags. Thus, as some of the X-ray radiation will be reflected quasi-instantaneously by the outer optical emitting disc, some radiation will be absorbed and re-emitted on the thermal time-scale. This would give rise to the broad optical lags observed. The reprocessing mechanism would also generate echoes within the optical light curve alone, with a delay close to the thermal time-scale.

ACKNOWLEDGEMENTS

SS acknowledges funding from the Alexander von Humboldt Foundation. GP acknowledges support by the Bundesministerium für Wirtschaft und Technologie/Deutsches Zentrum für Luft- und Raumfahrt (BMWI/DLR, FKZ 50 OR 1408) and the Max Planck Society. The authors also acknowledge Saul Rappaport and Daryll LaCourse for useful discussions relating to the *K2* light curve, as well as the anonymous referee for useful comments which have improved the manuscript. This research has made use of NASA's Astrophysics Data System Bibliographic Services. Additionally this work acknowledges the use of the astronomy & astrophysics package for MATLAB (Ofek 2014). This paper includes data collected by the *Kepler* mission. Funding for the *Kepler* mission is provided by the NASA Science Mission directorate. Some of the data presented in this paper were obtained from the Mikulski Archive for Space Telescopes (MAST). STScI is operated by the Association of Universities for Research in Astronomy, Inc, under NASA contract NAS5-26555. Support for MAST for non-*HST* data is provided by the NASA Office of Space Science via grant NNX13AC07G and by other grants and contracts. This research has made use of the MAXI data provided by RIKEN, JAXA and the MAXI team. This work is also based on observations obtained with the HERMES spectrograph, which is supported by the Fund for Scientific Research of Flanders (FWO), Belgium, the Research Council of K. U. Leuven, Belgium, the Fonds National de la Recherche Scientifique (F. R. S. – FNRS), Belgium, the Royal Observatory of Belgium, the Observatoire de Genve, Switzerland and the Thringer Landessternwarte Tautenburg, Germany.

REFERENCES

Afraimovich E. L., 1981, A&A, 97, 366
Arévalo P., Uttley P., 2006, MNRAS, 367, 801
Bildsten L., 1993, ApJ, 418, L21
Bogdanov S., Patruno A., Archibald A. M., Bassa C., Hessels J. W. T., Janssen J., Stappers B. W., 2014, ApJ, 789, 7
Bogert B., Healy M., Tukey J., 1963, in Rosenblatt M., ed., Proc. Symp. on Time Series Analysis: The Quefrency Alanysis of Time Series for Echoes: Cepstrum, Pseudo-Autocovariance, Cross-Cepstrum and Saphe Cracking. Wiley, New York, p. 209
Borucki W. J. et al., 2010, Science, 327, 977
Bradshaw C. F., Fomalont E. B., Geldzahler B. J., 1999, ApJ, 512, L121
Bradshaw C. F., Titarchuk L., Kuznetsov S., 2007, ApJ, 663, 1225
Britt C. T., 2013, PhD thesis, Louisiana State Univ.
Church M. J., Balucinska-Church M., 1995, A&A, 300, 441
Church M. J., Bałucińska-Church M., 2004, MNRAS, 348, 955
Church M. J., Gibiec A., Bałucińska-Church M., Jackson N. K., 2012, A&A, 546, A35
Cowley A. P., Crampton D., 1975, ApJ, 201, L65
Dieters S. W., van der Klis M., 2000, MNRAS, 311, 201
Edelson R. A., Krolik J. H., 1988, ApJ, 333, 646
Fender R. P., Russell D. M., Knigge C., Soria R., Hynes R. I., Goad M., 2009, MNRAS, 393, 1608
Giacconi R., Gursky H., Paolini F. R., Rossi B. B., 1962, Phys. Rev. Lett., 9, 439
Gottlieb E. W., Wright E. L., Liller W., 1975, ApJ, 195, L33
Hasinger G., van der Klis M., 1989, A&A, 225, 79
Hasinger G., van der Klis M., Ebisawa K., Dotani T., Mitsuda K., 1990, A&A, 235, 131
Heil L. M., Vaughan S., Uttley P., 2012, MNRAS, 422, 2620
Hertz P., Vaughan B., Wood K. S., Norris J. P., Mitsuda K., Michelson P. F., Dotani T., 1992, ApJ, 396, 201
Hjellming R. M. et al., 1990, ApJ, 365, 681
Hynes R. I., Britt C. T., 2012, ApJ, 755, 66
Kotov O., Churazov E., Gilfanov M., 2001, MNRAS, 327, 799
Lyubarskii Y. E., 1997, MNRAS, 292, 679
McNamara B. J. et al., 2003, AJ, 125, 1437
Matsuoka M. et al., 2009, PASJ, 61, 999
Mihara T. et al., 2011, PASJ, 63, 623
Mook D. E. et al., 1975, ApJ, 197, 425
Muñoz-Darias T., Martínez-Pais I. G., Casares J., Dhillon V. S., Marsh T. R., Cornelisse R., Steeghs D., Charles P. A., 2007, MNRAS, 379, 1637
Murray N., Chiang J., 1996, Nature, 382, 789
Ofek E. O., 2014, Astrophysics Source Code Library, record ascl:1407.005
Priedhorsky W., Hasinger G., Lewin W. H. G., Middleditch J., Parmar A., Stella L., White N., 1986, ApJ, 306, L91
Psaltis D., Lamb F. K., Miller G. S., 1995, ApJ, 454, L137
Raskin G. et al., 2011, A&A, 526, A69
Scaringi S., Körding E., Uttley P., Knigge C., Groot P. J., Still M., 2012, MNRAS, 421, 2854
Scaringi S., Körding E., Groot P. J., Uttley P., Marsh T., Knigge C., Maccarone T., Dhillon V. S., 2013, MNRAS, 431, 2535
Shakura N. I., Sunyaev R. A., 1973, A&A, 24, 337
Steeghs D., Casares J., 2002, ApJ, 568, 273
Sugizaki M. et al., 2011, PASJ, 63, 635
Timmer J., Koenig M., 1995, A&A, 300, 707
Uttley P., McHardy I. M., Vaughan S., 2005, MNRAS, 359, 345
Van de Sande M., Scaringi S., Knigge C., 2015, MNRAS, 448, 2430
van der Klis M., Swank J. H., Zhang W., Jahoda K., Morgan E. H., Lewin W. H. G., Vaughan B., van Paradijs J., 1996, ApJ, 469, L1
Vrtilek S. D., Raymond J. C., Garcia M. R., Verbunt F., Hasinger G., Kurster M., 1990, A&A, 235, 162
Vrtilek S. D., Penninx W., Raymond J. C., Verbunt F., Hertz P., Wood K., Lewin W. H. G., Mitsuda K., 1991, ApJ, 376, 278
Williams R. E., 1980, ApJ, 235, 939

This paper has been typeset from a TEX/LATEX file prepared by the author.